energies

MDPI

Article

A Novel Approach for the Determination of Sorption Equilibria and Sorption Enthalpy Used for MOF Aluminium Fumarate with Water

Eric Laurenz [1,2,*], Gerrit Füldner [1,*], Lena Schnabel [1] and Gerhard Schmitz [2]

[1] Department Heating and Cooling Technologies, Fraunhofer Institute for Solar Energy Systems ISE, Heidenhofstr. 2, 79110 Freiburg, Germany; lena.schnabel@ise.fraunhofer.de

[2] Institute of Engineering Thermodynamics, Hamburg University of Technology, Denickestr. 17, 21073 Hamburg, Germany; schmitz@tuhh.de

* Correspondence: eric.laurenz@ise.fraunhofer.de (E.L.); gerrit.fueldner@ise.fraunhofer.de (G.F.)

Received: 19 May 2020; Accepted: 9 June 2020; Published: 11 June 2020

Abstract: Adsorption chillers offer an environmentally friendly solution for the valorisation of waste or solar heat for cooling demands. A recent application is high efficiency data centre cooling, where heat from CPUs is used to drive the process, providing cooling for auxiliary loads. The metal organic framework aluminium fumarate with water is potentially a suitable material pair for this low temperature driven application. A targeted heat exchanger design is a prerequisite for competitiveness, requiring, amongst other things, a sound understanding of adsorption equilibria and adsorption enthalpy. A novel method is employed for their determination based on small isothermal and isochoric state changes, applied with an apparatus developed initially for volume swing frequency response measurement, to samples with a binder-based adsorbent coating. The adsorption enthalpy is calculated through the Clausius–Clapeyron equation from the obtained slopes of the isotherm and isobar, while the absolute uptake is determined volumetrically. The isotherm confirms the step-like form known for aluminium fumarate, with a temperature dependent inflection point at $p_{rel} \approx 0.25$, 0.28 and 0.33 for 30 °C, 40 °C and 60 °C. The calculated differential enthalpy of adsorption is 2.90 ± 0.05 MJ/kg (52.2 ± 1.0 kJ/mol) on average, which is about 10–15% higher than expected by a simple Dubinin approximation.

Keywords: adsorption equilibrium; adsorption enthalpy; heat of adsorption; metal organic framework; aluminum fumarate; coating; adsorption; cooling; heat pump; heat transformation

1. Introduction

Adsorption chillers offer an environmentally friendly solution for the valorisation of waste or solar heat for cooling demands. The working principle allows a simple, robust, and scalable design. Adsorption chillers and heat pumps have been applied successfully for different applications, like solar thermal cooling of buildings [1], gas adsorption heat pumps [2,3] and more [4,5]. A possible application that has attracted rising interest in recent years is the provision of data centre cooling driven by heat yielded from water cooled CPUs. Current high-performance CPUs allow cooling water temperatures of up to 60 °C or more [6,7], that can be used to drive adsorption chillers.

An adsorption chiller (Figure 1) consists of two adsorption heat exchangers, a condenser, and an evaporator, in a pure working fluid atmosphere. If temperatures below 0 °C can be excluded, usually water is used as working fluid, due to its high evaporation enthalpy. The adsorption heat exchangers (Ad-HX) have a heat transfer fluid on the primary and a stationary adsorbent material or composite on the secondary side. The process is cyclic: In the first half-cycle, the CPU's waste heat is used to regenerate the first Ad-HX. The desorbed working fluid is condensed in the condenser which is

cooled to the ambient at, e.g., 30 °C. In the second half-cycle, working fluid is adsorbed on the Ad-HX which, again, is cooled to the ambient. The resulting pressure drop induces the evaporation in the evaporator at about 20 °C, which is used to supply the air cooling of the server rooms. For continuous provision of cooling, two Ad-HXs are operated alternately. In contrast to typical thermally driven cooling applications, the coefficient of performance (COP) of this cycle is determined by the ratio of CPU and auxiliary heat loads and in the order of 0.5–0.6 [6].

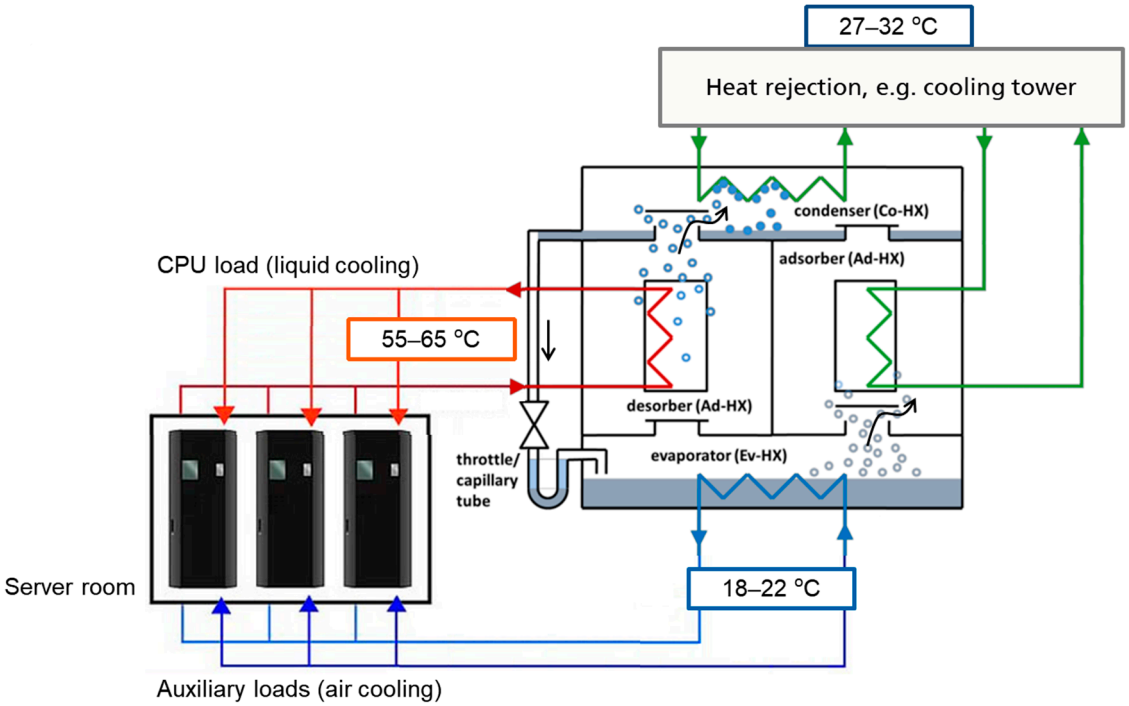

Figure 1. Working principle of an adsorption chiller for data centre cooling with typical feed and return temperature levels (schematic): high temperature CPU waste heat is yielded by direct water cooling and used to drive the adsorption chiller cycle, the chiller provides low temperature cooling for less temperature stable auxiliary loads (e.g., hard disks, power supplies), all heat flows are rejected at medium temperature level to the ambient, e.g., through a cooling tower.

The development of new adsorbent materials has been a research interest for many years [8]. Aluminium fumarate, a metal-organic framework (MOF) that attracted increasing interest for thermal applications in recent years, exhibits adsorption equilibrium properties that fit well to the boundary conditions of this cycle [9]. Due to its beneficial stepwise isotherm [8], it can allow considerably more efficient cycles compared to the state-of-the-art material silica gel with a good hydrothermal cycle stability [10,11]. Under the temperature conditions depicted in Figure 1, aluminium fumarate undergoes the full uptake step of about 0.3 kg/kg [10], compared to little more than 0.1 kg/kg for silica gel. This advantage may be used to reduce the amount of adsorbent or to increase the power density by, e.g., shorter cycles [12]. The material is potentially a low-cost material due to widely available educts (Al-salts and fumaric acid) and a water-based synthesis route [13].

The increase in volume specific cooling power (VSCP)—thus the reduction in specific costs—while keeping a reasonably high COP, is one of the major development challenges for adsorption chillers [12]. Typical values for COPs of market-available adsorption chillers are in the order of 0.5 to 0.65 [14]. In the case of data centre cooling, the target COP is determined by the ratio of low temperature cooling demand and available waste heat from CPUs, which typically is in the same range [6]. A promising approach to increase VSCP is to use binder-based adsorbent coatings to allow for a substantially better heat transfer to the heat exchanger structure, in comparison to a loose grain bed, the state-of-the-art solution [15]. Further performance increase can be reached through model-based design and optimisation, which is

more cost-effective than empiric trial-and-error prototyping, as shown recently in a comprehensive overview on designing strategies for Ad-HX by Graf et al. [16]. However, model-based design requires detailed knowledge of (a) the adsorption equilibria, (b) the adsorption enthalpy, (c) relevant physical heat and mass mechanisms and the corresponding transfer coefficients, and (d) the specific heat capacities, allowing for models with explicit dependency on design parameters like heat exchanger geometry, layer thicknesses and particle sizes. We developed a comprehensive approach to gain most of this data, i.e., (a)–(c), from small representative Ad-HX cut-outs in a single measurement procedure based on:

1. Volumetric uptake measurement;
2. Stepwise volume and temperature perturbation;
3. Frequency response analysis.

In this paper, we will focus on the first two steps for evaluating adsorption equilibrium and adsorption enthalpy. The frequency response analysis (FRA) for the investigation of heat and mass transfer processes builds upon this and will be dealt with in a following publication.

An apparatus developed initially for volume swing frequency response measurement also allows for measurements of the differential adsorption equilibrium, i.e., the slopes of the isotherm and the isobar, through the equilibrium response for small step experiments. Earlier, the FRA setups were used for volume step experiments to evaluate sorption dynamics, using a numerical non-linear transport model in the time domain [17], comparable to pressure jump [18,19] or temperature jump [20–22] experiments. We extend this approach to measuring the isobar slope with small temperature steps. Both slopes can be directly combined to determine the differential adsorption enthalpy at a specific thermodynamic state, i.e., adsorbent loading, temperature, and pressure. In combination with a calibrated dosing volume for the volumetric uptake measurement, this allows for a comprehensive determination of sorption equilibrium, enthalpy, and dynamics in a single automated measurement procedure.

2. Materials and Methods

2.1. Material

An aqueous dispersion (26.8 wt% aluminium fumarate (a.k.a. MIL-53(Al)-FA), Basolite® A520, BASF; 17.9 wt% SilRes® MP50E, Wacker Silicones) was processed by a knife coating applicator on 50 × 50 × 2 mm AlMg3 sample plates (Table 1). The wet film thickness was varied by an octagonal stainless-steel mask with a defined thickness (200 µm, 350 µm, 600 µm) and constant coating surface A_{ct} (18.7 cm^2). Samples were oven dried at 200 °C for 3 h before measuring coating thicknesses d_{ct} of final samples (Table 1, Figure 2) at five points with a probe indicator. The composite dry mass m_{cmp} was determined by quickly ($T \geq 160$ °C) weighing the hot samples under lab atmosphere after oven drying. Total dry adsorbent content $w_{s,dry}$ was first calculated from the suspension composition, based on experimentally determined dry masses of different components, as shown by Kummer et al. [23], and later cross checked by comparing the samples' uptake to the uptake of pure adsorbent powder measured volumetrically (AUTOSORB®, Quantachrome).

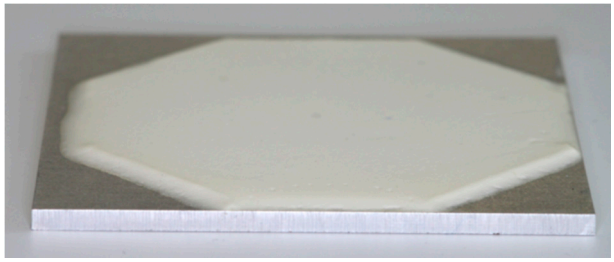

Figure 2. Sample Ct_610 with 0.61 mm coating thickness.

Table 1. Sample mass and geometry, the adsorbent content was estimated when mixing the coating suspension and confirmed later by comparing the sample's uptake with the pure adsorbent powder isotherm (c.f. Section 3.1).

				By Suspension Composition		By Comparison to Pure Adsorbent Uptake	
Sample	m_{cmp}**(mg)**	d_{ct}**(mm)**	ρ_{cmp} **(g/cm³)**	$w_{s,dry}$**(-)**	w_{bnd}**(-)**	$w_{s,dry}$ **(-)**	w_{bnd}**(-)**
Ct_140	134 ± 3	0.14 ± 0.04	0.51 ± 0.15	0.75	0.25	0.72	0.28
Ct_240	217 ± 4	0.24 ± 0.05	0.48 ± 0.10	0.75	0.25	0.79	0.21
Ct_610	563 ± 11	0.61 ± 0.07	0.49 ± 0.06	0.75	0.25	0.80	0.20

2.2. Apparatus

Measurements are performed with a custom setup (Figure 3, Table 2) under pure water vapour atmosphere, allowing vapour dosing as well as small volume and temperature steps. Moreover, the setup allows frequency response (FR), large temperature jump (LTJ), large pressure jump (LPJ) and small pressure jump (SPJ) experiments with water. Details on jump experiments with the setup have been reported extensively before [20,24,25], FR experiments will be published elsewhere.

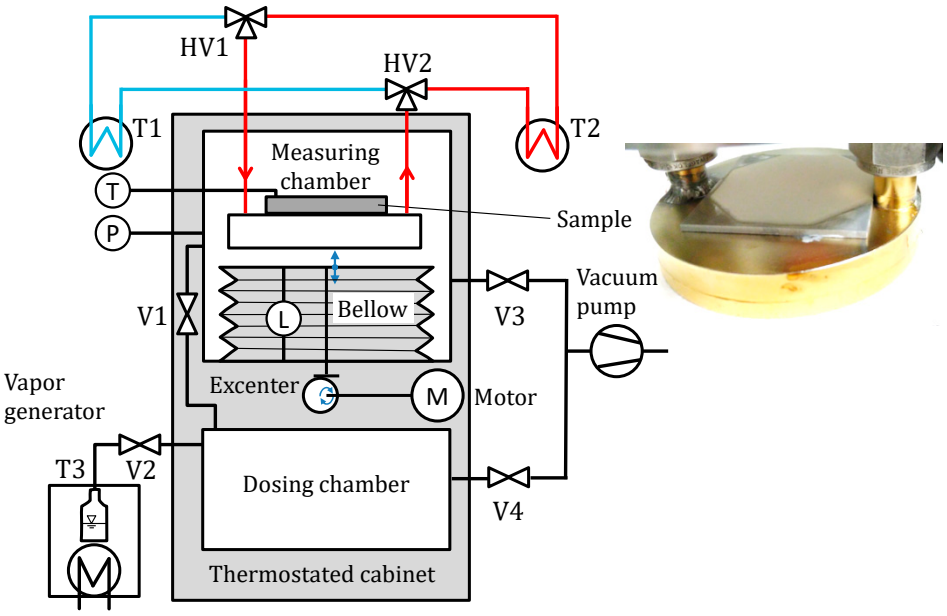

Figure 3. Sorption kinetic setup for frequency response, large temperature jump and large pressure jump experiments with absolute and differential equilibrium measurement. Absolute sorption equilibria are measured volumetrically by dosing in from the dosing chamber, differential equilibria by small temperature and pressure steps around equilibrium.

Table 2. Principal characteristics of measurement quantities, details are explained in the text.

Quantity	**Range**	**Typical Uncertainty**	**Device**
Chamber volume	849–922 mL	0.4 mL (20 °C), 1.3 mL (80 °C)	Schreiber Messtechnik LVDT
Chamber pressure	0–100 mbar	0.05 mbar (5 mbar), 0.15 mbar (100 mbar)	MKS Baratron 627B
Cold plate temperature	20–95 °C	0.1 K	4-wired Pt100
Sample surface temperature	20–80 °C	Not applicable [1]	Heitronics KT15

[1] The sample surface temperature is used to qualitatively ensure steady state conditions.

The volume of the dosing chamber is constant ($V_D = 41.815 \pm 0.021$ L), while the measurement chamber volume ($\overline{V}_M = 885.4 \pm 1.3$ mL) can be varied by 4.12% through a mechanically driven vacuum bellow, while the bellow position is recorded with a vacuum stable linear variable differential transformer (LVDT, Schreiber Messtechnik). The bellow position has been calibrated with a second order polynomial to the chamber volume by filling the evacuated and temperature-controlled chamber with water of known mass. The sample is thermally well connected (thermal grease TG20032) to the cold plate kept isothermal (±0.01 K) by two switchable external circuits. The cold plate temperature is precisely measured with a 4-wired Pt100 sensor embedded in a bore. The chamber pressure is measured with a capacitive pressure transducer (MKS Baratron 627B, 0–100 mbar). Additionally, the sample's surface temperature is recorded using an IR temperature sensor (Heitronics KT15) through a ZnSe vacuum viewport with a noise equivalent temperature difference of 25 mK at a response time of 1 s. The measurement spot has a diameter of 6 mm (95%) and the detector's spectral response maximum is between 8 and 14 µm, fitting to the transmissivity of the ZnSe viewport and the aimed sample temperature (20–80 °C). To minimise temperature gradients, the whole vacuum setup is encapsulated in a temperature-controlled cabinet (±0.1 K) set to the mean cold plate temperature. Data acquisition is performed with a high precision digital multimeter (Agilent 34970A).

2.3. Procedure

The measurement procedure consists of two steps: pre-conditioning to the desired state and determination of equilibrium slopes. Throughout the measurement, the temperature-controlled cabinet is kept at the measurement mean temperature T_0.

Initially, samples were desorbed against a rotary vane pump ($p < 0.01$ mbar) at 95 °C overnight, to remove any co-adsorbed impurities. For aluminium fumarate this ensures an initial loading X_{init} of 0 kg/kg. After cooling down the closed chamber to T_0, the sample is pre-conditioned to a desired loading X_0 by dosing in vapour from the dosing chamber. X_0 is calculated volumetrically from the mass balance of both chambers and the adsorbent dry mass $m_s = w_{s,dry} m_{cmp}$ following the ideal gas law, which is a very good approximation for water in the pressure and temperature region of the measurements:

$$X_0 = X_{init} + \frac{1}{T_0 R_w m_s}[V_D p_{D1} + V_{M1} p_{M1} - (V_{M2} p_{M2} + V_D p_{D2})]. \quad (1)$$

Here, indexes D and M denote the dosing and the measurement chamber where the volume depends on the bellow position, and indexes 1 and 2 denote the equilibrium state before and after dosing in vapour. The pressures $p_{D,1}$ and $p_{D,2}$ are calculated beforehand based on the isotherm of the pure adsorbent powder to approximately reach the set point for X_0. The equilibrium pressure of the sample $p_0 = p_{M,2}$ will follow the equilibrium of the sorbent at T_0 and X_0, yielding a point on the T_0-isotherm. To calculate the effective loading X_{eff}, the composite mass, m_{cmp} is used in Equation (1) instead of m_s.

To determine the equilibrium slopes at the pre-conditioned sample state, the sample is exposed to small volume and temperature jumps symmetrically around V_0 and T_0, first by $\Delta V = 2\hat{V}$ with constant temperature and then by $\Delta T = 4$ K with constant volume. This allows determining the differential equilibrium, i.e., the slopes of the isotherm $dX/dp \approx (\Delta X/\Delta p)_T$ and the isobar $dX/dT \approx ((\Delta X - dX/dp \Delta p)/\Delta T)_V$ from the equilibrium pressure difference Δp and loading change ΔX, measured for the isothermal and the isochoric jump, respectively. A very slow drift in the pressure, which is due to parasitic effects of the setup already reported [24,25], is corrected by fitting linear models to equilibrium sections before and after the jump and using the extrapolated values at the centre. Finally, with both slopes the differential enthalpy of adsorption at X_0 and T_0 can be calculated based on the Clausius–Clapeyron equation assuming ideal gas behaviour:

$$\Delta h_s \approx \frac{RT^2}{p}\frac{dp}{dT} = -\frac{RT^2}{p}\frac{dX}{dT}\left(\frac{dX}{dp}\right)^{-1} \quad (2)$$

Loading, differential equilibrium and adsorption enthalpy are important input parameters for a subsequent FRA reported elsewhere. Integration in a single measurement routine allows for measurement under exactly the same conditions (in-situ). As the sample is pre-conditioned only once, this eliminates the need for time consuming external measurements and possibly error-prone transfer to the measurement conditions.

To exclude a local hysteresis of the adsorption equilibrium, an important pre-requisite for FRA, a further test is included in the routine: The same equilibrium state X_0, T_0 is reached coming from a smaller and a larger volume at constant temperature and vice versa. The equilibrium loading is then compared and a "hysteresis-free" behaviour assumed if the loading difference between the two directions is below the measurement uncertainty.

2.4. Uncertainty Evaluation

Uncertainty analysis has been carried out based on GUM [26], including uncertainty from sample variance (type A) and uncertainties from imperfect calibration and correction (type B).

The uncertainty of the mean values are between 0.4 mL (20 °C) and 1.3 mL (80 °C) for V_0, between 0.05 mbar ($p_0 = 5$ mbar) and 0.15 mbar ($p_0 = 100$ mbar) for the chamber pressure, and about 0.1 K for the mean sample temperature T_0. Typical uncertainties for vapour dosing are in the order of 1 to 4 mg influenced mainly by p_0 for 10 to 60 mbar. Thus, uncertainties for the loading are smaller for higher sample dry mass, given constant dry mass uncertainty.

3. Results and Discussion

Results are reported for five different loadings at 40 °C and one loading at 30 °C and 60 °C, respectively.

3.1. Adsorption Equilibrium

The water isotherm of the adsorbent powder at 40 °C (Figure 4) shows the characteristic step-like uptake to a plateau at 0.32 kg/kg and is in line with [11], or slightly lower than [10,27] previous results. The position of the step is temperature dependent with an inflection point at $p_{rel} \approx 0.25$, 0.28 and 0.33 for 30, 40 and 60 °C. Measured local isotherm slopes are in agreement with the tangent for 40 °C. The position of the uptake step is reproducible within the samples and shows a strong temperature dependency that persists when applying a Dubinin transformation [28]. Hence, the assumption of a temperature invariant characteristic curve is a strong simplification for aluminium fumarate and should be applied with care. The exact position of the uptake step is an important information for application, as it determines the available driving forces and finally the resulting equipment power [3].

No significant hysteresis was observed, neither locally by the procedure explained before, in Section 2.3, nor globally. For the latter, the vapour dosing procedure was modified starting with a saturated sample ($p_{rel} = 0.5$, $T = 40$ °C, $X_{init} = 0.33$ kg/kg$_s$) and desorbing into the dosing chamber. The hysteresis found in previous results was probably due to incomplete equilibrium and/or pore condensation occurring at $p_{rel} \gg 0.5$, which was disregarded here due to the limited relevance for heat transformation applications.

The adsorbent content calculated by comparing the uptake of the sample to that of the powder (Figure 4, right), fits on average the values calculated at sample preparation (Table 1), showing that the binder has no significant influence on adsorption equilibrium. The results show good agreement between the two thicker samples and a slight deviation of the thinnest sample Ct_140, which could be explained by a slightly lower adsorbent content of the coating. The difference to the uptake of the pure adsorbent can be explained by the inert binder/loss due to the coating process, differences in the production process and measurement uncertainty of the volumetric adsorption measurement.

A general description of the measured sorption equilibrium for modelling purposes is given in the Supplementary Material (S1).

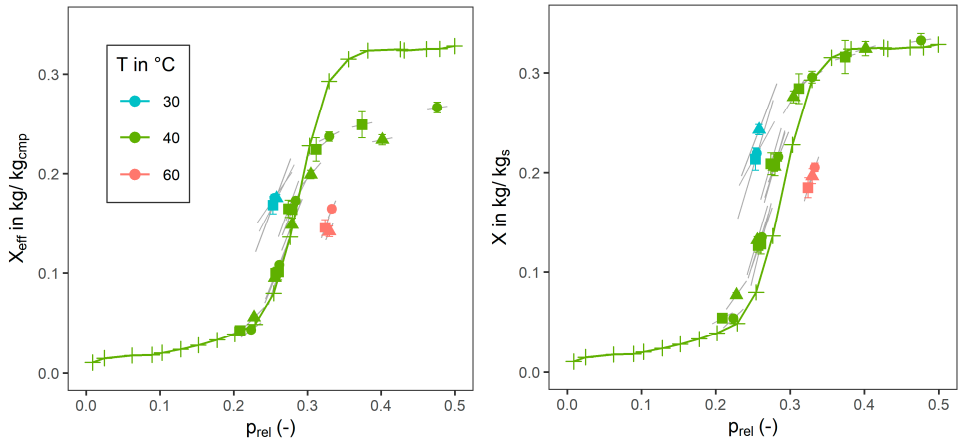

Figure 4. Effective loading X_{eff} and loading $X = X_{\text{eff}}/w_{\text{s,dry}}$ over relative pressure measured for samples Ct_140 (▲), Ct_240 (■), and Ct_610 (●) in comparison with the 40 °C isotherm of the pure adsorbent powder (+), adsorbent content $w_{\text{s,dry}}$ determined by uptake correction; grey lines: local equilibrium slope measured by small volume jumps.

3.2. Adsorption Enthalpy

The calculated differential enthalpy of adsorption is 2.90 ± 0.05 MJ/kg (52.2 ± 1.0 kJ/mol) on average. The calculation with Equation (2) is based on either the local equilibrium slope indicated in Figure 5 or on a linear fit of the quasi-isosteric points ($X_{\text{eff}} \approx 0.16$ kg/kg) measured at 30, 40 and 60 °C. The Clausius–Clapeyron plot shows that local slopes coincide well with the multi-temperature fit, and so do the calculated enthalpies. Temperature and loading dependencies are negligible in the parameter range evaluated. The adsorption enthalpy is about 10–15% higher than expected by a simple Dubinin approximation (sum of evaporation enthalpy at the same temperature and the adsorption potential $A = -RT\ln(p_{\text{rel}})$, [28]), which is in qualitative accordance to the observed temperature variance of the isotherm. Thus, the application of the concepts of a characteristic curve to describe the sorption equilibrium, and of the adsorption potential to describe the sorption enthalpy, results in a rather crude approximation for the case of aluminium fumarate.

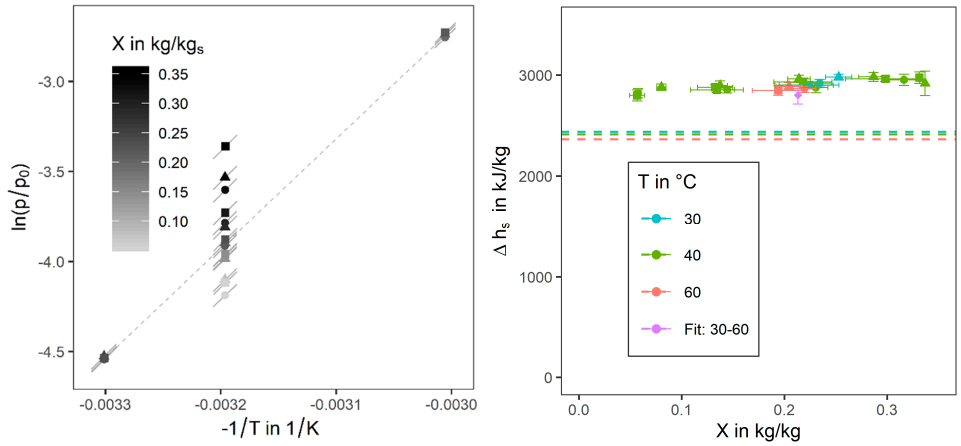

Figure 5. Left: Clausius–Clapeyron plot ($p_0 = 1$ bar) with measured equilibrium points for different samples (▲ Ct_140, ■ Ct_240, ● Ct_610) and isostere slope calculated from measured local deviations (short grey lines) and linear fit of points with $X_{\text{eff}} \approx 0.16$ kg/kg (- - -), uncertainties of T and p are bellow point size; Right: differential adsorption enthalpy calculated from isostere slopes of local equilibria and 0.2-kg/kg-fit over corrected loading with the evaporation enthalpy of water (- - -).

4. Conclusions

In this work we developed a novel method for in-situ measurements of sorption equilibria and enthalpy, in an apparatus dedicated to the sorption dynamic measurement. The method, based on dosing vapour from calibrated volumes and small temperature and volume steps around an equilibrium point, allows for direct measurements of the isobar's and isotherm's slope, tightly around a specific thermodynamic state. This allows extracting the loading and temperature dependency of the isostere's slope and thus the sorption enthalpy.

The method was tested on samples coated with a composite of aluminium fumarate particles with Silres® as a binder, in different thicknesses (140–610 µm) at 30–60 °C and the entire loading range. The measured sorption equilibrium fits expectations from the pure adsorbent powder's isotherm and the coating composition. The coating procedure did not alter the adsorption properties.

The measurement of the differential adsorption enthalpy was successfully verified by comparing the local slope of the isostere to the linear regression over the whole temperature range. The sorption enthalpy is 2.90 ± 0.05 MJ/kg (52.2 ± 1.0 kJ/mol) on average, with no significant dependency with either loading or temperature.

Supplementary Materials: The following are available online at http://www.mdpi.com/1996-1073/13/11/3003/s1, Section S1: General description of the sorption equilibrium of aluminium fumarate.

Author Contributions: Conceptualization, E.L. and G.F.; methodology, E.L.; software, E.L.; validation, G.F. and L.S.; formal analysis, E.L.; investigation, E.L.; resources, E.L.; data curation, E.L.; writing—original draft preparation, E.L.; writing—review and editing, G.F., L.S. and G.S.; visualization, E.L.; supervision, G.F., L.S. and G.S.; project administration, G.F.; funding acquisition, E.L., G.F., L.S. and G.S. All authors have read and agreed to the published version of the manuscript.

Funding: This work results widely from the PhD project of Eric Laurenz for which funding by Heinrich Böll Stiftung is gratefully acknowledged. In addition, funding by BMBF for project WasserMod2 (FKZ 03ET1554A) is gratefully acknowledged.

Acknowledgments: The authors would like to thank Harry Kummer for supervising and Raffael Wolf for carrying out the sample preparation, Phillip Hügenell for performing the AUTOSORB® measurement, and Florian Tönnies for implementing parts of the data processing program.

Conflicts of Interest: The authors declare no conflict of interest.

Nomenclature

Abbreviations

Ad-HX	Adsorber heat exchanger

Variables

T	Temperature (K)
p	Pressure (Pa)
X	Loading ($kg_{adsorbed}/kg_{sorbent,dry}$)
X_{eff}	Effective loading ($kg_{adsorbed}/kg_{composite,dry}$)
V	Volume (m^3)
A	Surface area (m^2), adsorption potential (J/kg), Amplitude (any unit)
R	Universal gas constant (J/(mol K))
R_w	Specific gas constant of water (J/(kg K))
m	Mass (kg)
t	Time (s)
M	Molar mass (kg/mol)
Δh_s	Differential adsorption enthalpy ($J/kg_{adsorbed}$)

Indices

w	Water
s	(Ad)sorbent, (ad)sorption
0	Temporal mean value
D	Dosing chamber
M	Measurement chamber

V	At constant volume
T	At constant temperature
ch	(Measurement) chamber
cmp	Composite
ct	Coating
rel	Relative

References

1. Meunier, F. Adsorption heat powered heat pumps. *Appl. Therm. Eng.* **2013**, *61*, 830–836. [CrossRef]
2. Metcalf, S.J.; Critoph, R.E.; Tamainot-Telto, Z. Optimal cycle selection in carbon-ammonia adsorption cycles. *Int. J. Refrig.* **2012**, *35*, 571–580. [CrossRef]
3. Wittstadt, U.; Füldner, G.; Laurenz, E.; Warlo, A.; Große, A.; Herrmann, R.; Schnabel, L.; Mittelbach, W. A novel adsorption module with fiber heat exchangers: Performance analysis based on driving temperature differences. *Renew. Energy* **2017**, *110*, 154–161. [CrossRef]
4. Wang, D.C.; Li, Y.H.; Li, D.; Xia, Y.Z.; Zhang, J.P. A review on adsorption refrigeration technology and adsorption deterioration in physical adsorption systems. *Renew. Sustain. Energy Rev.* **2010**, *14*, 344–353. [CrossRef]
5. Pang, S.C.; Masjuki, H.H.; Kalam, M.A.; Hazrat, M.A. Liquid absorption and solid adsorption system for household, industrial and automobile applications: A review. *Renew. Sustain. Energy Rev.* **2013**, *28*, 836–847. [CrossRef]
6. Wilde, T.; Ott, M.; Auweter, A.; Meijer, I.; Ruch, P.; Hilger, M.; Kuhnert, S.; Huber, H. CooLMUC-2: A supercomputing cluster with heat recovery for adsorption cooling. In *Thirty-third Annual Semiconductor Thermal Measurement and Management Symposium, Proceedings of 2017 33rd Thermal Measurement, Modeling & Management Symposium (SEMI-THERM), San Jose, CA, USA, 13–17 March 2017*; Wesling, P., Ed.; IEEE: Piscataway, NJ, USA, 2017; pp. 115–121. ISBN 978-1-5386-1531-7.
7. Zimmermann, S.; Meijer, I.; Tiwari, M.K.; Paredes, S.; Michel, B.; Poulikakos, D. Aquasar: A hot water cooled data center with direct energy reuse. *Energy* **2012**, *43*, 237–245. [CrossRef]
8. Aristov, Y.I. Challenging offers of material science for adsorption heat transformation: A review. *Appl. Therm. Eng.* **2013**, *50*, 1610–1618. [CrossRef]
9. Lenzen, D.; Zhao, J.; Ernst, S.-J.; Wahiduzzaman, M.; Ken Inge, A.; Fröhlich, D.; Xu, H.; Bart, H.-J.; Janiak, C.; Henninger, S.; et al. A metal-organic framework for efficient water-based ultra-low-temperature-driven cooling. *Nat. Commun.* **2019**, *10*, 3025. [CrossRef] [PubMed]
10. Jeremias, F.; Fröhlich, D.; Janiak, C.; Henninger, S.K. Advancement of sorption-based heat transformation by a metal coating of highly-stable, hydrophilic aluminium fumarate MOF. *RSC Adv.* **2014**, *4*, 24073–24082. [CrossRef]
11. Kummer, H.; Jeremias, F.; Warlo, A.; Füldner, G.; Fröhlich, D.; Janiak, C.; Gläser, R.; Henninger, S.K. A Functional Full-Scale Heat Exchanger Coated with Aluminum Fumarate Metal–Organic Framework for Adsorption Heat Transformation. *Ind. Eng. Chem. Res.* **2017**, *56*, 8393–8398. [CrossRef]
12. Schnabel, L.; Füldner, G.; Velte, A.; Laurenz, E.; Bendix, P.; Kummer, H.; Wittstadt, U. Innovative Adsorbent Heat Exchangers: Design and Evaluation. In *Innovative Heat Exchangers*; Bart, H.J., Scholl, S., Eds.; Springer International Publishing: Cham, Switzerland, 2018; pp. 363–394. ISBN 978-3-319-71641-1.
13. Kiener, C.; Müller, U.; Schubert, M. Organometallic Aluminum Fumerate Backbone Material. PCT/EP2007/053567, 9 April 2009.
14. ASUE. Marktübersicht Gaswärmepumpen 2017/18. Available online: https://asue.de/sites/default/files/asue/themen/gaswaermepumpe_kaelte/2017/broschueren/ASUE_Marktuebersicht-Gaswaermepumpen_2017.pdf (accessed on 6 February 2019).
15. Freni, A.; Dawoud, B.; Bonaccorsi, L.; Chmielewski, S.; Frazzica, A.; Calabrese, L.; Restuccia, G. Adsorption Heat Exchangers. In *Characterization of zeolite-based coatings for adsorption heat pumps*; Freni, A., Ed.; Springer: Cham, Switzerland, 2015; pp. 35–53. ISBN 978-3-319-09326-0.
16. Graf, S.; Eibel, S.; Lanzerath, F.; Bardow, A. Validated Performance Prediction of Adsorption Chillers: Bridging the Gap from Gram-Scale Experiments to Full-Scale Chillers. *Energy Technol.* **2020**, 1901130. [CrossRef]

17. Bourdin, V.; Gray, P.G.; Grenier, P.; Terrier, M.F. An apparatus for adsorption dynamics studies using infrared measurement of the adsorbent temperature. *Rev. Sci. Instrum.* **1998**, *69*, 2130–2136. [CrossRef]
18. Schnabel, L.; Tatlier, M.; Schmidt, F.; Erdem-Şenatalar, A. Adsorption kinetics of zeolite coatings directly crystallized on metal supports for heat pump applications (adsorption kinetics of zeolite coatings). *Appl. Therm. Eng.* **2010**, *30*, 1409–1416. [CrossRef]
19. Frazzica, A.; Füldner, G.; Sapienza, A.; Freni, A.; Schnabel, L. Experimental and theoretical analysis of the kinetic performance of an adsorbent coating composition for use in adsorption chillers and heat pumps. *Appl. Therm. Eng.* **2014**, *73*, 1022–1031. [CrossRef]
20. Velte, A.; Füldner, G.; Laurenz, E.; Schnabel, L. Advanced Measurement and Simulation Procedure for the Identification of Heat and Mass Transfer Parameters in Dynamic Adsorption Experiments. *Energies* **2017**, *10*, 1130. [CrossRef]
21. Graf, S.; Lanzerath, F.; Sapienza, A.; Frazzica, A.; Freni, A.; Bardow, A. Prediction of SCP and COP for adsorption heat pumps and chillers by combining the large-temperature-jump method and dynamic modeling. *Appl. Therm. Eng.* **2016**, *98*, 900–909. [CrossRef]
22. Aristov, Y.I.; Dawoud, B.; Glaznev, I.S.; Elyas, A. A new methodology of studying the dynamics of water sorption/desorption under real operating conditions of adsorption heat pumps: Experiment. *Int. J. Heat Mass Transf.* **2008**, *51*, 4966–4972. [CrossRef]
23. Kummer, H.; Füldner, G.; Henninger, S.K. Versatile siloxane based adsorbent coatings for fast water adsorption processes in thermally driven chillers and heat pumps. *Appl. Therm. Eng.* **2015**, *85*, 1–8. [CrossRef]
24. Füldner, G. Stofftransport und Adsorptionskinetik in porösen Adsorbenskompositen für Wärmetransformationsanwendungen. Ph.D. Thesis, Universiät Freiburg, Freiburg, Germany, 2015.
25. Schnabel, L. Experimentelle und numerische Untersuchung der Adsorptionskinetik von Wasser an Adsorbens-Metallverbundstrukturen. Ph.D. Thesis, Technische Universität Berlin, Berlin, Germany, 2009.
26. JCGM. *Guide to the Expression of Uncertainty in Measurement (GUM 1995 with Minor Corrections)*; Joint Committee for Guides in Metrology, JCGM: Sèvres, France, 2008; Volume 100.
27. Elsayed, E.; AL-Dadah, R.; Mahmoud, S.; Elsayed, A.; Anderson, P.A. Aluminium fumarate and CPO-27(Ni) MOFs: Characterization and Thermodynamic Analysis for Adsorption Heat Pump Applications. *Appl. Therm. Eng.* **2016**. [CrossRef]
28. Dubinin, M.M.; Astakhov, V.A. Description of Adsorption Equilibria of Vapors on Zeolites over Wide Ranges of Temperature and Pressure. In *Molecular Sieve Zeolites. 2: International Conference on Molecular Sieves 2*; Flanigen, E.M., Sand, L.B., Eds.; American Chemical Society: Washington, DC, USA, 1971; pp. 69–85. ISBN 0-8412-0115-3.

© 2020 by the authors. Licensee MDPI, Basel, Switzerland. This article is an open access article distributed under the terms and conditions of the Creative Commons Attribution (CC BY) license (http://creativecommons.org/licenses/by/4.0/).